Chapter 6

NLTE vs. LTE

6.1 Abstract

We finish up this thesis with a look at the first word in the title, 'NLTE'. NLTE stands for non-local thermodynamic equilibrium. It basically represents all processes which can effect the level populations of an ionic species which can not be explained by the local temperature through the Saha and Boltzmann equations. This includes both the impinging radiation field and non-thermal ionization. Our focus will be concentrated in two areas. First, how does using an LTE approximation (in contrast with a reasonably full NLTE calculation) effect the resultant model. Second, what do the NLTE calculations tell us about the features in the spectra. In the end we wish to convince the reader of the necessity of performing NLTE calculations and their usefulness in the interpretation of the spectra of SNe Ia near maximum light.

6.2 Differences

To explore the differences between LTE and NLTE calculations we will look no further than the W7 model at 20 days which is seen in Chapter 5. This calculation has (by particle number) the majority of the atmosphere in NLTE. Most importantly it has both Fe II and Co II in NLTE which not only have several strong lines in the spectra of SNe Ia but also have a large number of weaker lines (in the millions) which, taken as a group, control the overall shape of the spectra. This model was calculated with a nebular inner-boundary condition. The two LTE models which we consider do not incorporate this inner-boundary condition. These models also make use of a constant scattering albedo, $\alpha = 0.1$.

Model	$\mathrm{M_{bol}}$	M_U	M_B	M_V	M_R
NLTE	-18.71	-19.12	-18.93	-18.94	-18.83
LTE #1	-18.78	-19.37	-18.92	-18.92	-18.84
LTE #2	-18.38	-18.62	-18.46	-18.69	-18.61

Table 6.1: Magnitudes for the NLTE and LTE models.

In Figure 6.1 we see a plot of the NLTE calculation vs. two LTE models. Table 6.1 lists the UBVRI and bolometric magnitudes for each. What should stick out immediately is how neither LTE model correctly reproduces the colors in the NLTE model, even though they span a large range in absolute bolometric magnitude. Model LTE #1 is clearly to bright in the UV while it matches the optical rather well up to 7000 Å. LTE #2 is a decent match in the far UV (up to 3500 Å) though it is very underluminous in the optical and IR. The reason behind this can be seen in Figure 6.2. Here the percentage temperature difference between each LTE model and the NLTE model is plotted vs. velocity. Bracketing a 5% range in temperature difference one can see that LTE #1 is a better match at lower velocities (5,000 to 12,500 km/s) and LTE #2 matches better at higher velocities (12,500 to 25,000 km/s). Since the UV is optically thick until the very outer regions of the atmosphere, it makes sense that the model which matches temperature structure better in this range, LTE #2, will fit the spectrum better in the UV. Likewise, the optical part of the spectrum (since it becomes thin at much lower velocities) will be

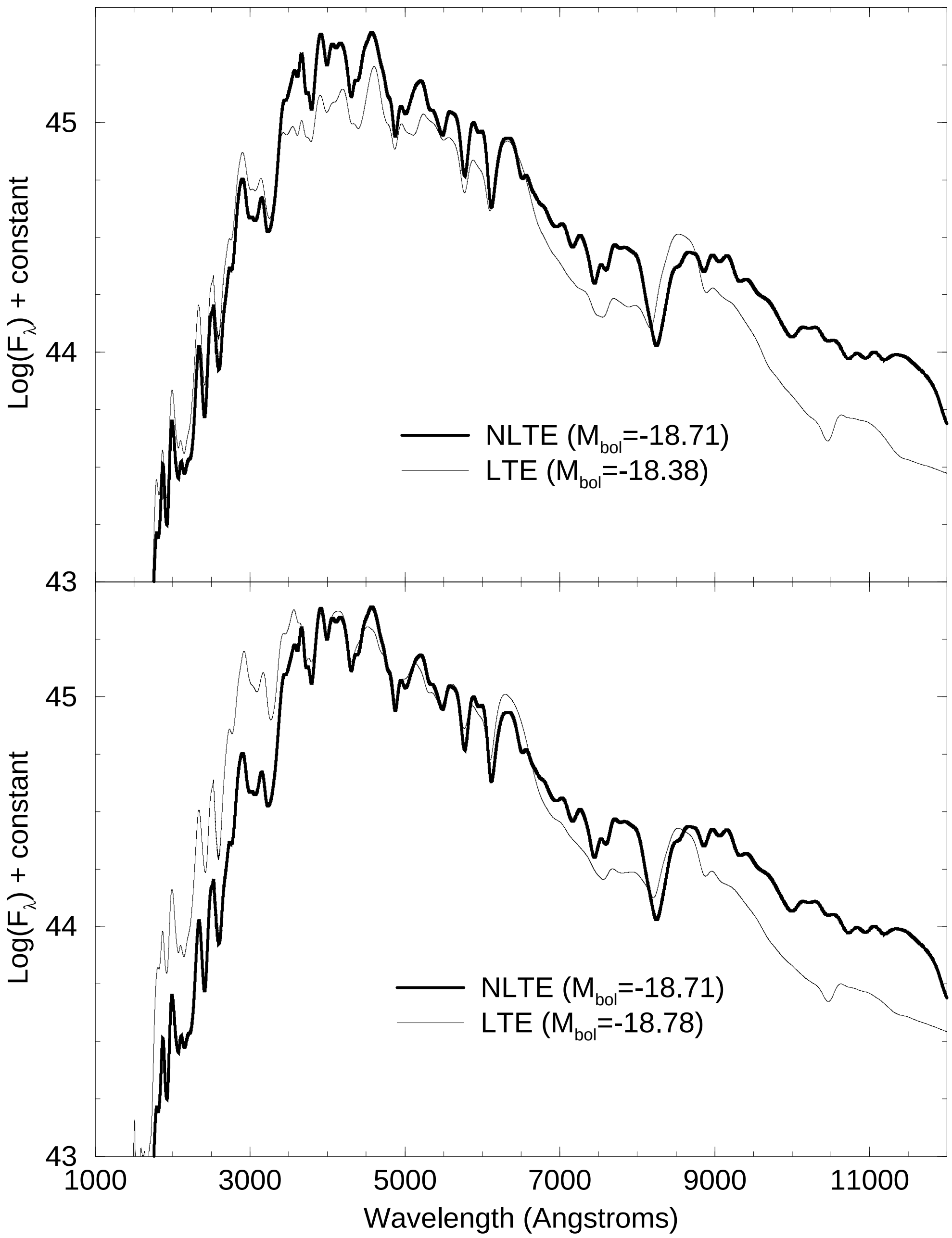

Figure 6.1: A comparison of LTE and NLTE spectra.

better matched by model LTE #1, since it more correctly matches the temperature structure at depth.

In Figure 6.3 we present the b_i's for the strongest lines for each element in the optical region of the spectrum. The transitions considered (labeled by their approximate wavelengths) are as follows: C I – 9100 Å, O I – 7780 Å, Mg II – 4490 Å, S II – 5650 Å, Si II – 6350 Å, Ca II – 3940 Å, Fe II – 5180 Å and Co II – 4170 Å. The b_i's (as we present them here) are the ratio of the NLTE level populations to the LTE level populations given the NLTE ionization. It is quite obvious from this figure that most of the species are far from LTE, even at depth. Of particular note is the O I line which is far from LTE everywhere in the atmosphere and was impossible to fit in our earlier models where we considered it only in LTE (see Nugent et al. (1995a)). One can also see how Si II departs far from LTE (especially at depth). This feature is especially important for SNe Ia since it's spectral signature is used to classify these events.

6.3 Line Identifications

We end the thesis with a brief section on line identification in SNe Ia. While several strong lines are readily apparent in the near maximum light spectra, it will become quite obvious from the next few graphs that, in general, a spectrum's shape and features are controlled by the blending of many thousands (even millions) of weak lines. This is especially true of the iron peak elements.

Figures 6.4 through 6.8 display the sum of the Sobolev optical depths, in 10 Å̃bins, for each ionic species throughout the line forming region. The wavelengths have been blueshifted by 10,000 km/s (roughly the photospheric velocity) in order to match up better with the major features in the synthetic spectra rather than being at the

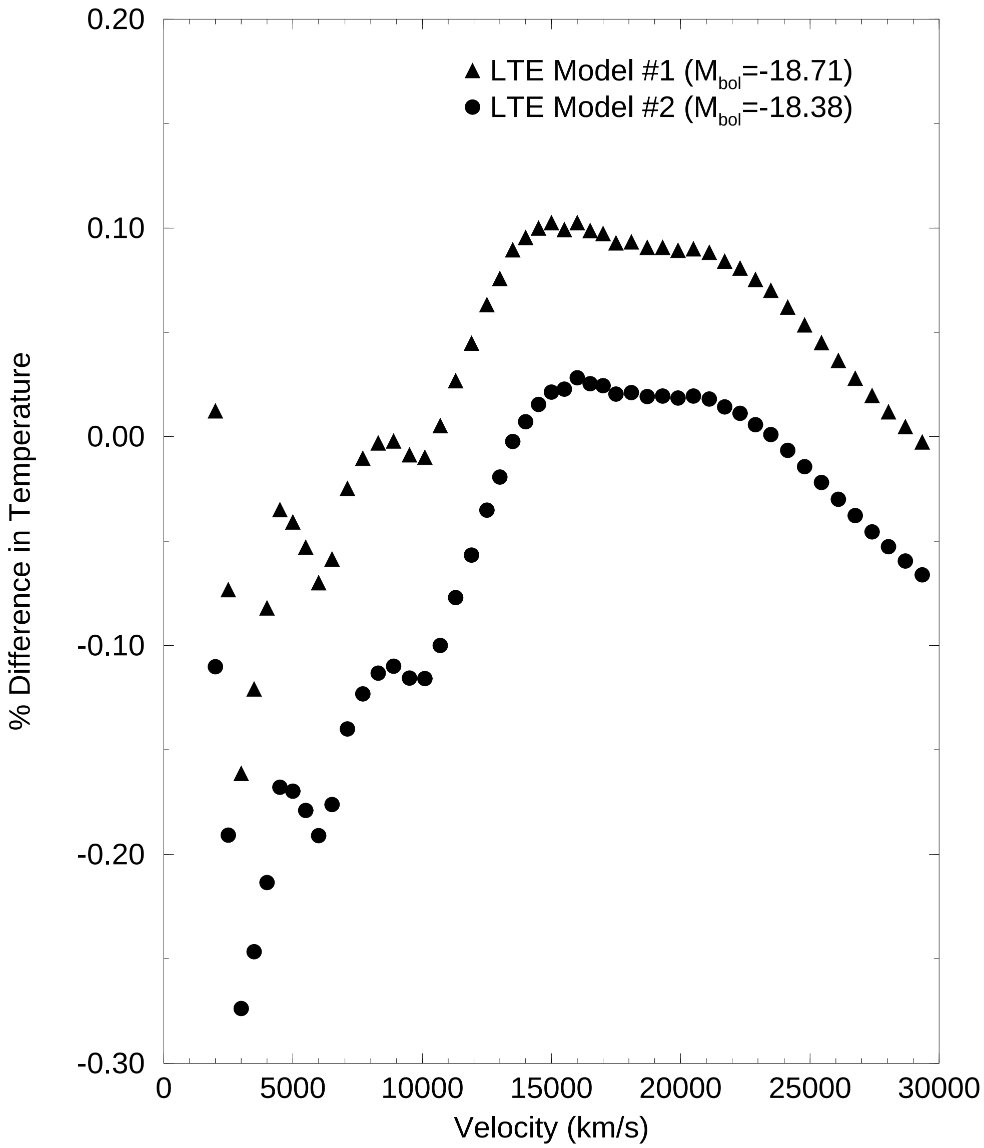

Figure 6.2: The percentage difference in temperature between the NLTE and LTE spectra.

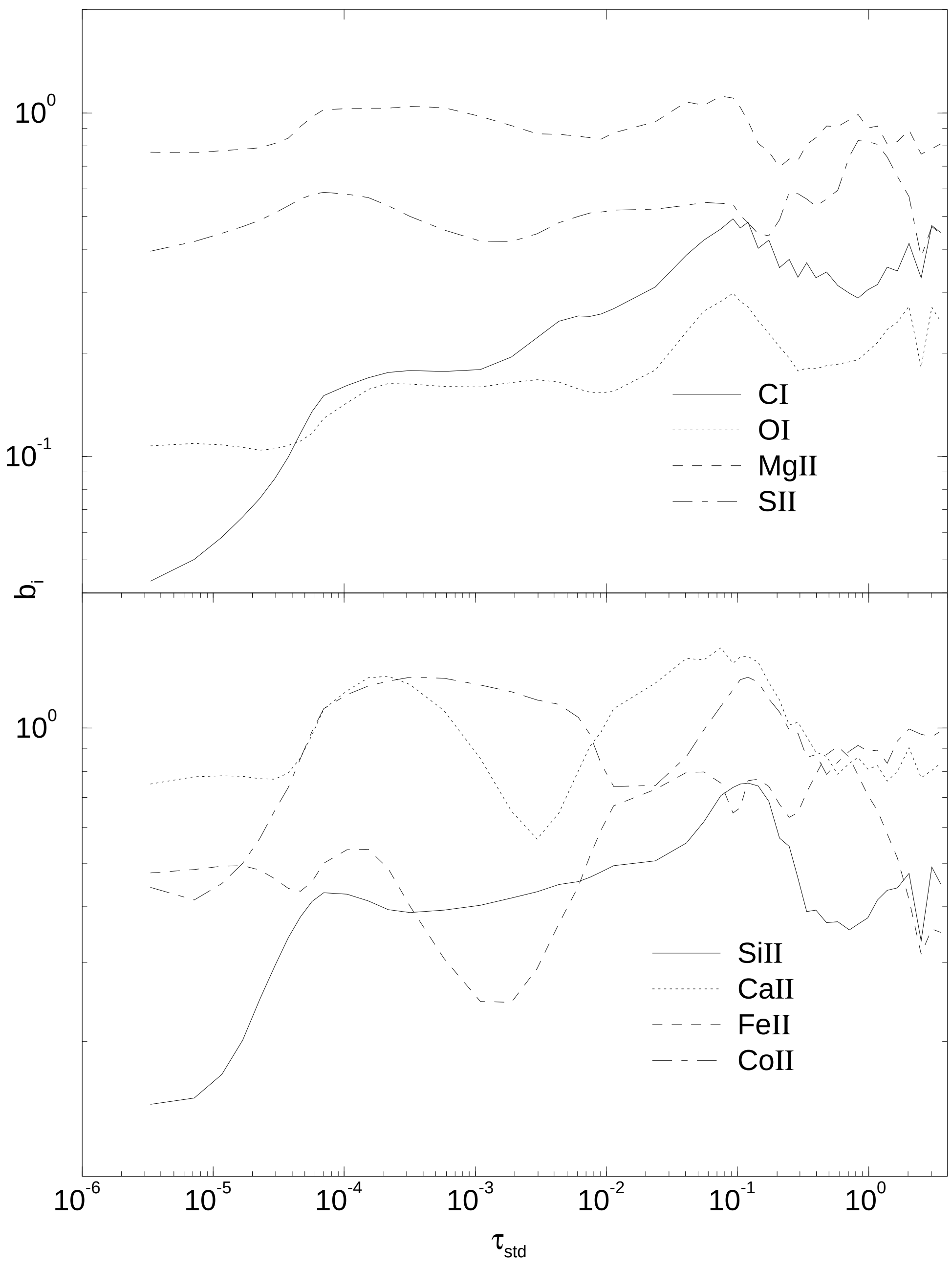

Figure 6.3: The b_i's for the NLTE model. The transitions considered are as follows: C I – 9100 Å, O I – 7780 Å, Mg II – 4490 Å, S II – 5650 Å, Si II – 6350 Å, Ca II – 3940 Å, Fe II – 5180 Åand Co II – 4170 Å.

rest wavelength. All the standard line identifications stick out tremendously having optical depths approaching 10^{6-7}. One can easily match up the strong features associated with the Ca II H&K lines and infrared triplet, the Si II features at either side of 6000 Å (though note how Na I makes its presence known in the bluer of the lines), the S II 'W' feature at 5400 Å and the several strong Mg II features stretching from 2800 Å to the near infrared.

The major players though are Ti II, Fe II and Co II. Their presence in the UV is what directly controls the overall shape of the spectrum. The line blanketing they produce in the UV is what takes a relatively Planckian spectrum in the IR and optical and hacks it off at 4000 Å. In addition, one can see that Fe II is strong throughout the entire spectrum with Sobolev optical depths greater than 10^2 all the way to 1.0 μ. In future work we will examine how the strengths of these features change as a function of time and overall luminosity, paying particular attention to the Ti II lines near 4400 Å which make a much stronger appearance in the dimmer SNe Ia.

In conclusion, we have demonstrated both the necessity and usefulness of performing NLTE spectrum synthesis calculations of SNe Ia. We have shown how these calculations can be used for abundance determinations and line identifications, the acceptance or rejection of a particular model and as an independent (and purely physical-based) way to determine the distance to a supernova. Though the work in this field is far from complete, this thesis has made great strides into the analysis of SNe Ia and has provided a means to tackle many of the remaining questions.

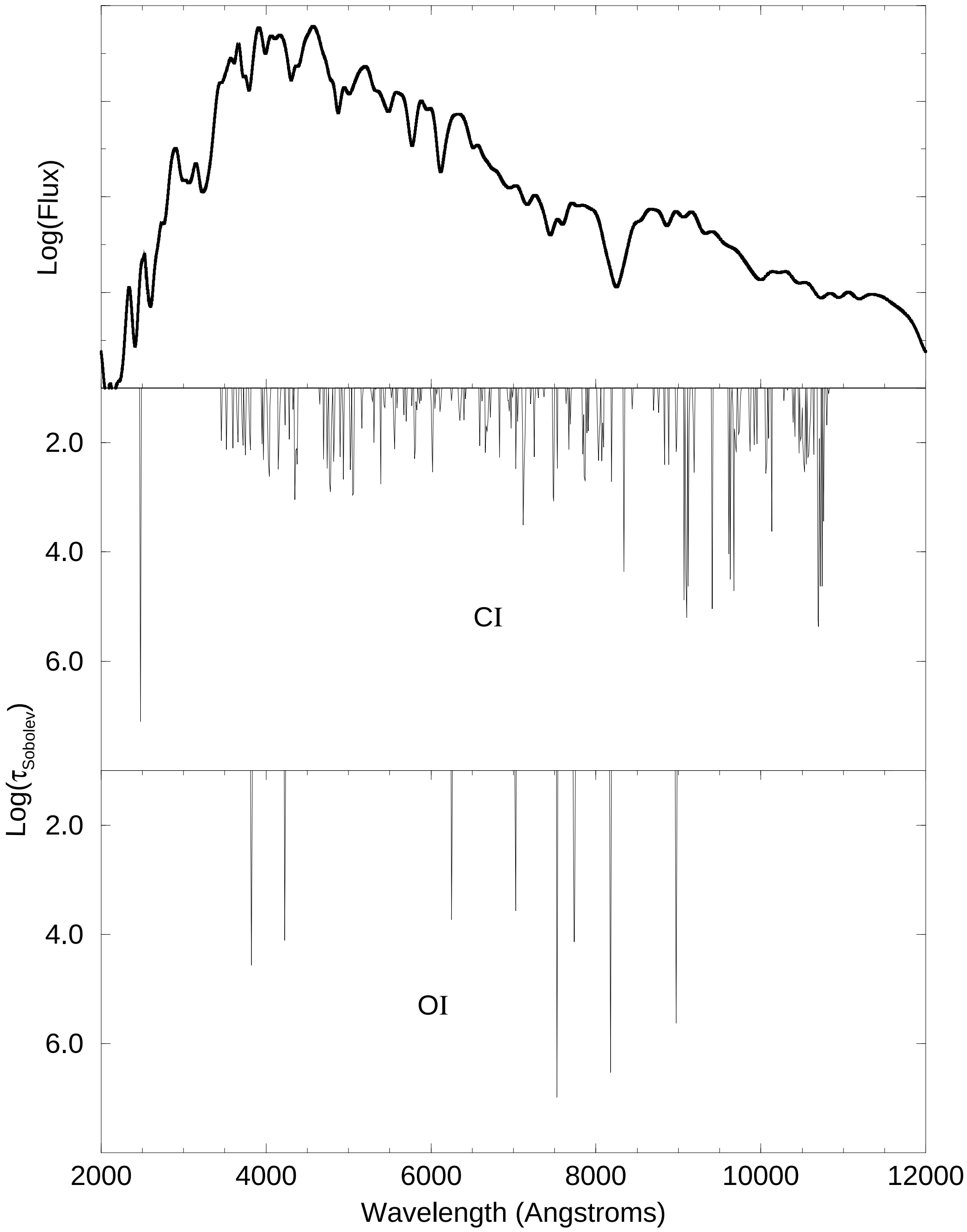

Figure 6.4: The Sobolev optical depths for O I and C I throughout the line forming region in the atmosphere.

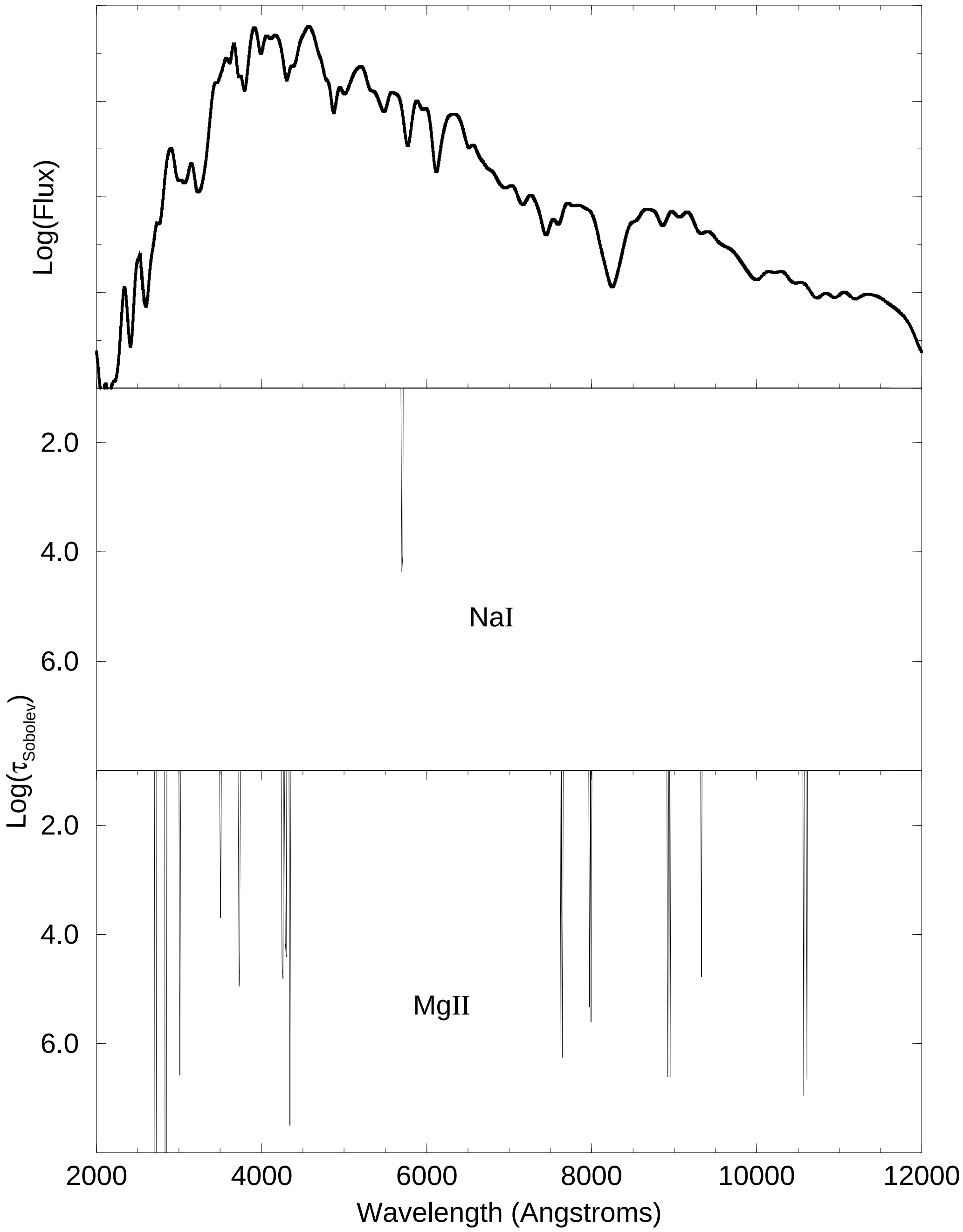

Figure 6.5: The Sobolev optical depths for Na I and Mg II throughout the line forming region in the atmosphere.

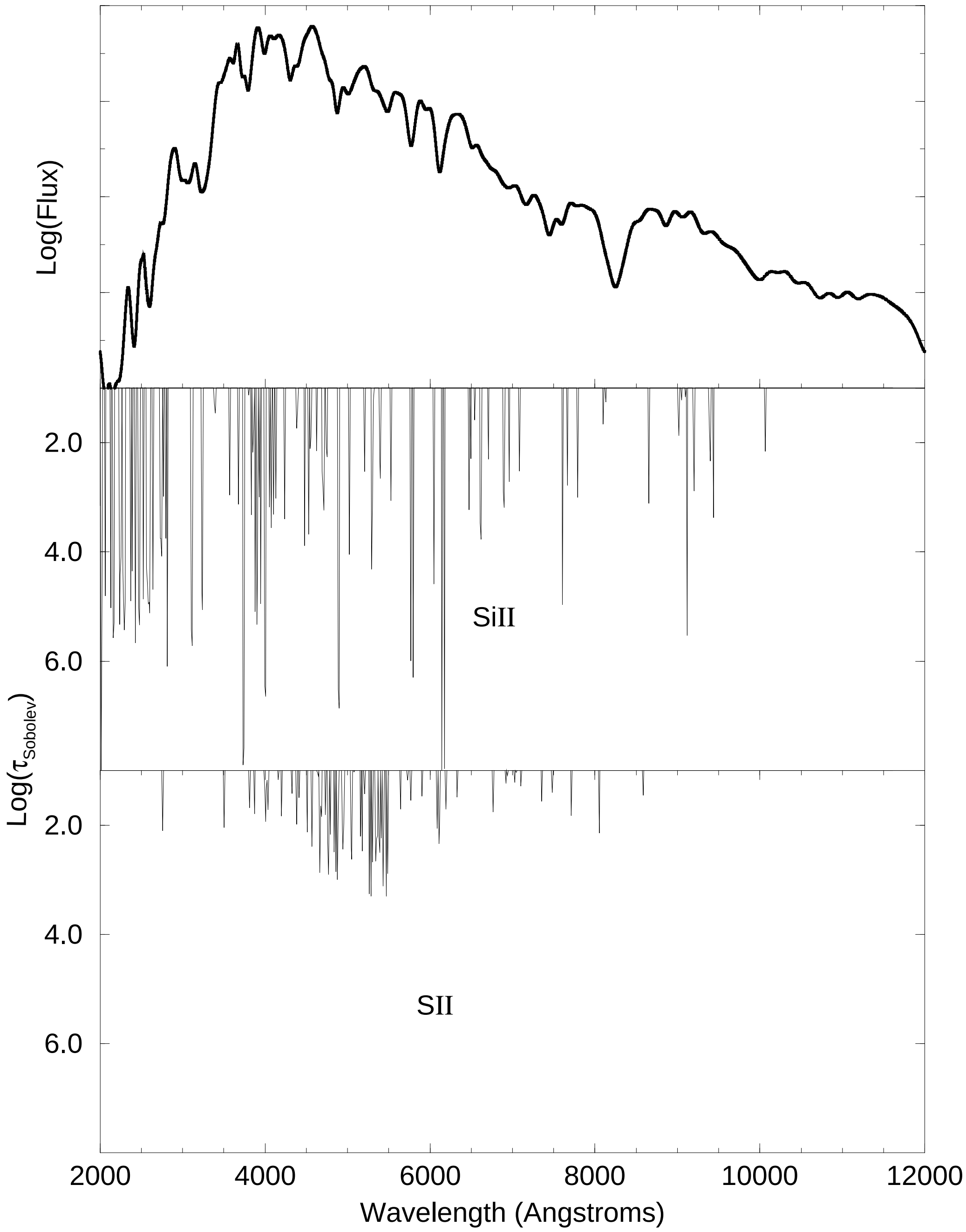

Figure 6.6: The Sobolev optical depths for Si II and S II throughout the line forming region in the atmosphere.

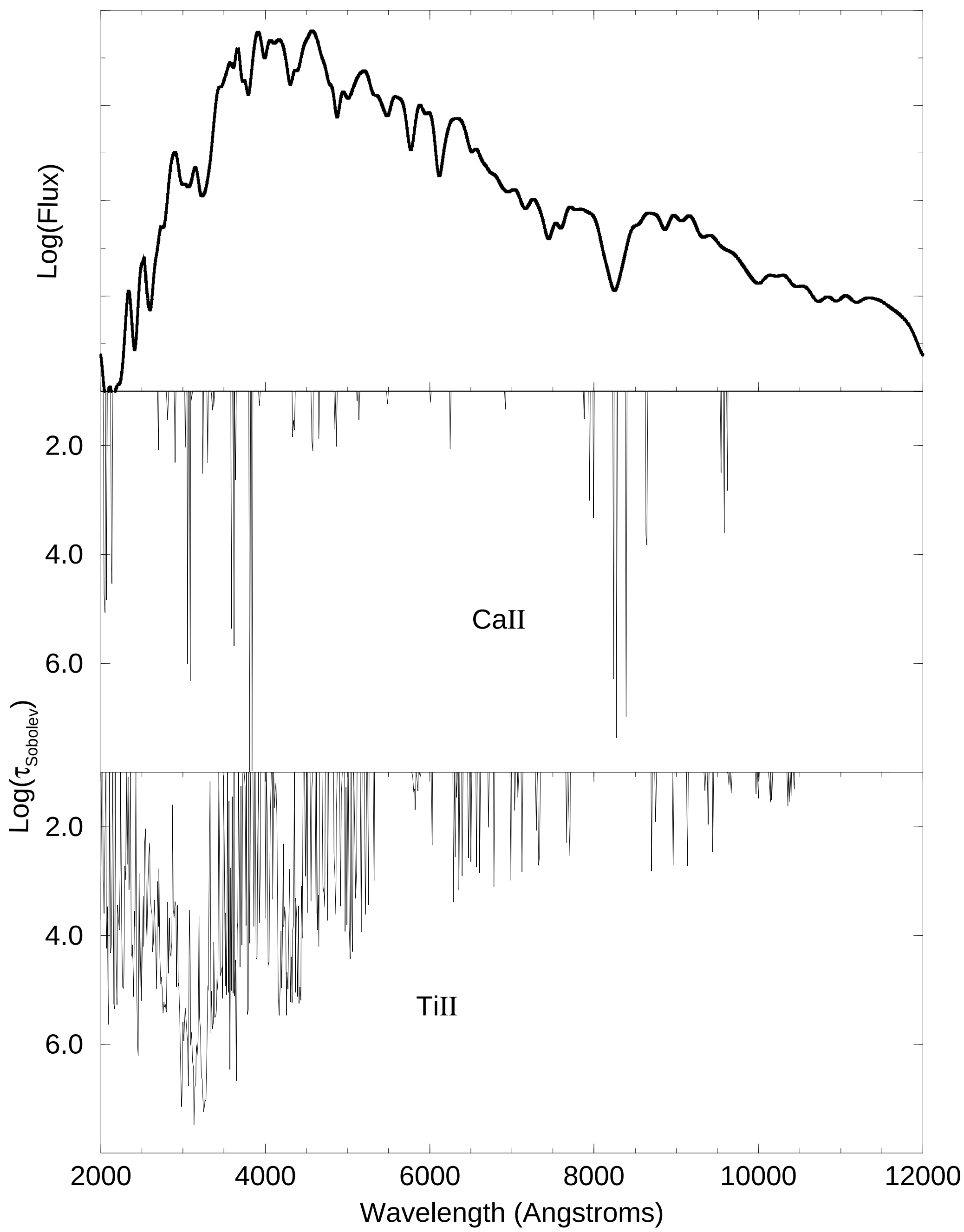

Figure 6.7: The Sobolev optical depths for Ca II and Ti II throughout the line forming region in the atmosphere.

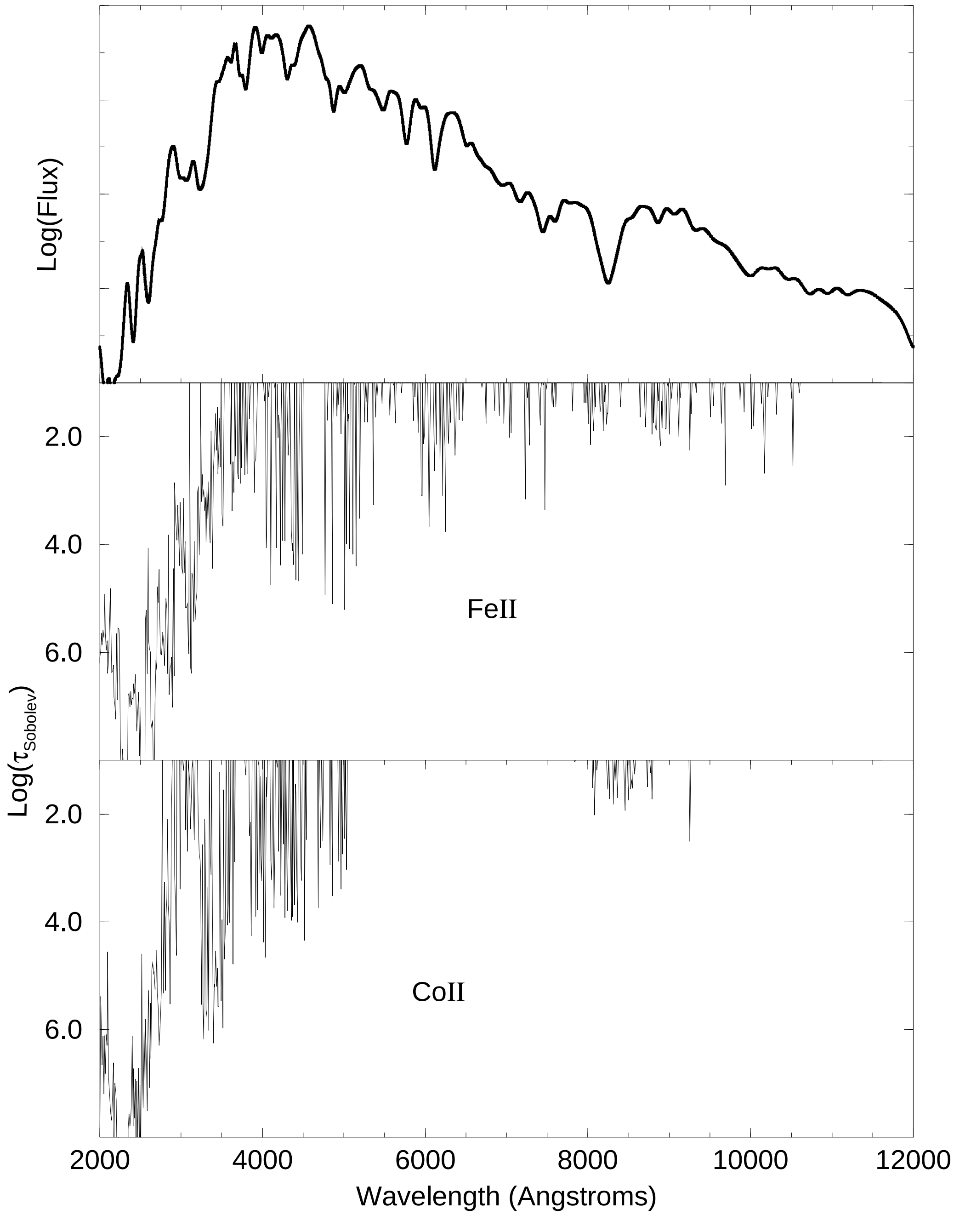

Figure 6.8: The Sobolev optical depths for Fe II and Co II throughout the line forming region in the atmosphere.